

# Fiber Optical Detection of Lithium Plating at Graphite Anodes

Jonas Hedman, Ronnie Mogensen, Reza Younesi, and Fredrik Björefors\*

Avoiding the plating of metallic lithium on the graphite anode in lithium-ion batteries, potentially leading to aging and the formation of dendrites is critical for long term and safe operation of the cells. In this contribution, in operando detection of lithium plating via a fiber optical sensor placed at the surface of a graphite electrode is demonstrated. The detection is based on the modulation of light at the sensing region, which is in direct contact with the graphite particles. This is first demonstrated by the intentional deposition of lithium on a copper electrode, followed by experiments with graphite electrodes in pouch cells where plating is initiated both as a result of over-lithiation and excessive cycling rates. The plating resulted in a significant loss of light from the fiber, and the findings correlated well with previous experiments on the detection of sodium plating. The modulated light is also found to correlate well with the graphite staging via changes in the optical properties of the graphite during slow (de) intercalation of lithium ions. In a practical application, the fiber optical sensor may provide a battery management system (BMS) with input to optimize the charging procedure or to warn for cell failure.

improve the understanding of chemical reactions in the cells.

Sensors based on optical fibers are particularly well suited to be incorporated into battery cells.<sup>[1,7,9–12]</sup> The fibers are of low cost and can be made very thin, enabling precise positioning in different parts of the batteries. They are also relatively inert to the harsh environment in lithium- and sodium-ion batteries, and a wide range of analysis techniques based on spectroscopy are available.<sup>[7]</sup> Sensing via changes in the temperature and strain in the cells, indirectly affecting the optical properties of modified fibers, has also been demonstrated. Huang et al., for example, inserted fiber optical Bragg gratings into commercial cells to follow chemical events via the temperature and pressure,<sup>[10]</sup> while Wang et al. employed plasmonic fiber optical sensors to monitor electrochemical kinetics in aqueous zinc air batteries.<sup>[11]</sup> Ghannoum

## 1. Introduction

A wide variety of relatively small, cheap, and relatively simple sensors are presently being developed for in-operando use in modern batteries.<sup>[1–4]</sup> The aim is to obtain important information from the cells that could provide input to a BMS,<sup>[5]</sup> in addition to the current, voltage, and temperature. The sensors, which could be placed both inside and outside of the cells, are, for example, expected to deliver a better estimate of the state of charge (SOC), optimize the use of the cells, and warn of harmful reactions or even catastrophic events. Some common examples include sensors based on acoustics,<sup>[6]</sup> optics,<sup>[7]</sup> and strain.<sup>[8]</sup> The sensors are also intended to function as research tools for the development of new anode and cathode materials, as well as to

et al. have in a number of papers reported the use of fiber-optic evanescent wave (FOEW) spectroscopy for the characterization of cells.<sup>[9,13]</sup> An embedded optical fiber was for example used to estimate the SOC based on the electrochromic properties of graphite.<sup>[14]</sup> We have also previously employed FOEW spectroscopy to compare the sensing and battery performances for optical fibers either fully embedded or placed at the surface of lithium iron phosphate (LFP) cathodes. In those experiments, the modulation of the light at the sensing region of the fiber could also be linked to the oxidation and reduction of iron in the LFP.<sup>[15,16]</sup> Incorporation of optical fibers in batteries is still at a rather low technology readiness level and may not be trivial in commercial cells, but has the potential to provide a BMS with important information for the optimized use of a battery pack. In general, the knowledge of how cell chemistry modulates the light at the fiber/battery interface must also be improved.

One of the most critical safety aspects of lithium-ion batteries is the risk of formation of lithium dendrites at the anode.<sup>[17–19]</sup> These can lead to a short circuit in the cell and is typically originating from lithium plating when the rate of lithium-ion intercalation is not sufficient during charging. Plating of metallic lithium is also one important factor leading to the aging<sup>[17]</sup> of cells, for example resulting in an increased rate of capacity fade. A wide range of experimental techniques has been employed to analyze and detect lithium plating.<sup>[17–19]</sup> The majority of these techniques are, however, based on large, advanced, and expensive instrumentation that often requires specialized experimental cells or prototype batteries. Some of them are also not

J. Hedman, R. Mogensen, R. Younesi, F. Björefors  
Department of Chemistry – Ångström Laboratory  
Uppsala University  
Box 538, SE-751 21 Uppsala, Sweden  
E-mail: fredrik.bjorefors@kemi.uu.se

 The ORCID identification number(s) for the author(s) of this article can be found under <https://doi.org/10.1002/admi.202201665>.

© 2022 The Authors. Advanced Materials Interfaces published by Wiley-VCH GmbH. This is an open access article under the terms of the Creative Commons Attribution License, which permits use, distribution and reproduction in any medium, provided the original work is properly cited.

DOI: 10.1002/admi.202201665

suited for in operando evaluations as they rely on post-mortem analysis. A small and relatively inexpensive sensor inside a battery that can detect lithium plating is hence a promising alternative to optimize the charging conditions and to warn for possible growth of dendrites while using the battery in a practical application. In addition, many efforts have been dedicated to reducing or controlling the lithium plating in intercalation batteries.<sup>[20]</sup> Rehnlund et al.<sup>[21]</sup> further suggested that short lithium nucleation pulses to increase the lithium nuclei density on the electrode surface to mitigate problems with dendrite formation on lithium metal anodes. Such efforts may also benefit from sensors capable of analyzing the lithium plating.

We have also previously demonstrated the use of FOEW spectroscopy for the detection of sodium plating on hard carbon anodes, both as a result of insufficient capacity and excessive charging rates.<sup>[22]</sup> It was found that the intensity output from the sensor decreased significantly at the onset of sodium plating and that the cell performance was not significantly affected by the presence of an optical fiber. In the present work, we demonstrate the direct detection of lithium plating on graphite in pouch cells using the same optical fiber sensors, both as a result of over-lithiation and excessive cycling rates. In addition, we also show the possibility to follow the lithium staging in graphite during slow (de)intercalation of lithium ions. Overall, the results show that the wavelength-dependent

information from the sensor could be used as a warning sign for lithium plating.

## 2. Results and Discussion

### 2.1. Lithium Plating on Copper

To first demonstrate the detection of lithium plating, the FOEW sensor was placed directly on top of a bare copper disk functioning as the working electrode (WE) in a half-cell. Lithium metal was electrochemically deposited on the copper by using a constant current of  $-0.123 \text{ mA cm}^{-2}$ , and the plating and the following stripping step were limited to 30 min each. The resulting potential profiles are shown in Figure 1a and the corresponding optical response is in Figure 1b. As lithium was plated on the copper electrode (discharge of the cell), there was a sharp drop in intensity for all wavelengths, with the intensity decreasing more for the longer wavelengths. Figure 1c,d demonstrates the potential profiles and optical response during the first few minutes in more detail. Following the initial reduction of the electrolyte at the start of the experiment, the potential of the WE rapidly dropped below 0 V versus  $\text{Li}^+/\text{Li}$  and there was also a clear sign of a nucleation dip, indicating lithium plating (marked with a dashed line in Figure 1c). Furthermore,

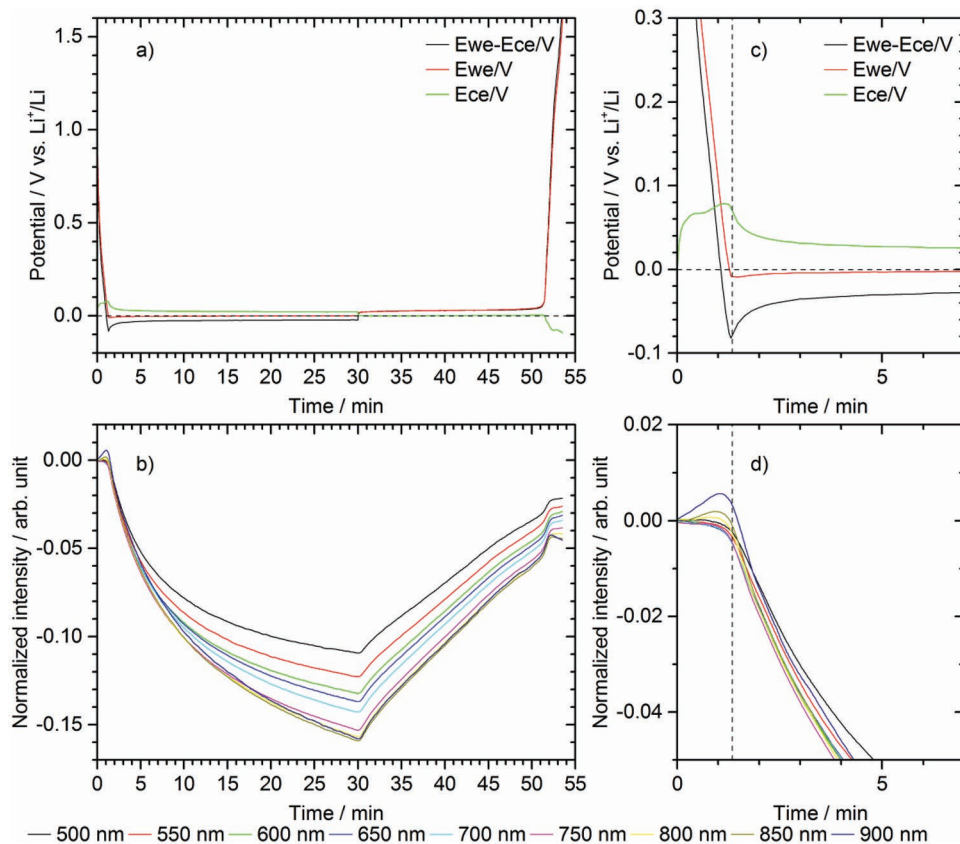


**Figure 1.** Lithium plating and stripping in a copper (WE) and lithium (CE) half-cell with a piece of lithium included as a reference electrode. The plating was induced by using a constant current of  $-0.123 \text{ mA cm}^{-2}$  (corresponding to a rate of C/20 for a graphite electrode of equal dimensions). The voltage profiles are shown in (a) and the corresponding intensity in (b). Zoomed-in figures are provided in (c) and (d), where the vertical dashed line is positioned at the lithium nucleation dip.

also note the peculiar voltage profile of the counter electrode (CE) in the first few minutes and the following overpotential ( $\approx 20\text{--}30\text{ mV}$ ), originating from surface contaminations of the Li metal CE as discussed in A. Mohammadi et al.<sup>[23]</sup> What is also clear from the optical response in Figure 1d is the small increase in intensity for the longer wavelengths (800–900 nm) prior to the plating.

The significant drop in intensity from the fiber optical sensor upon lithium plating was hence found to be very similar to previous experiments on sodium plating on a copper electrode of equal size and with comparable current density.<sup>[22]</sup> Likewise, the wavelength dependence was almost fulfilled after  $\approx 30\text{ min}$ , and the small increase in the intensity for the longer wavelengths prior to the lithium plating was also present in the previous sodium plating experiments.<sup>[22]</sup>

When a positive current was applied after 30 min to oxidize the deposited lithium, the optical response was reversed with a distinct increase in intensity at all wavelengths (Figure 1b). This was expected since the lithium was stripped from the copper. Furthermore, from the result in Figure 1, it can be concluded that the plating and stripping efficiency of lithium on copper (using a carbonate-based electrolyte) were rather low, as the intensity after the stripping step did not reach the same

level as at the start of the experiment. This indicates that some lithium remained passivated<sup>[22]</sup> on either the copper substrate or was caught in the separator. From post-mortem analysis of the copper electrode, it was apparent that significant amounts of lithium metal remained on the electrode after several plating and stripping cycles (see Figure S1, Supporting Information).

## 2.2. Plating on Lithiated Graphite

To demonstrate the light modulation from lithium plating on graphite, a similar experiment was designed where the copper was replaced by a graphite electrode having an area capacity of  $2.46\text{ mAh cm}^{-2}$ . The experiment was carried out by first performing four formation cycles at 0.1 C with the lower cut-off potential set to 5 mV (vs the lithium reference electrode), followed by a slow lithiation and intentional plating at C/20 (terminated after 30 h). Figure 2a,b shows the potential profiles during lithiation and delithiation, respectively, for the graphite during a formation cycle, and the maximum capacity reached approximately  $300\text{ mAh g}^{-1}$ . From the potentials, the steps representing the lithium staging<sup>[24]</sup> in graphite were clearly seen. The corresponding change in intensity from the fiber optical

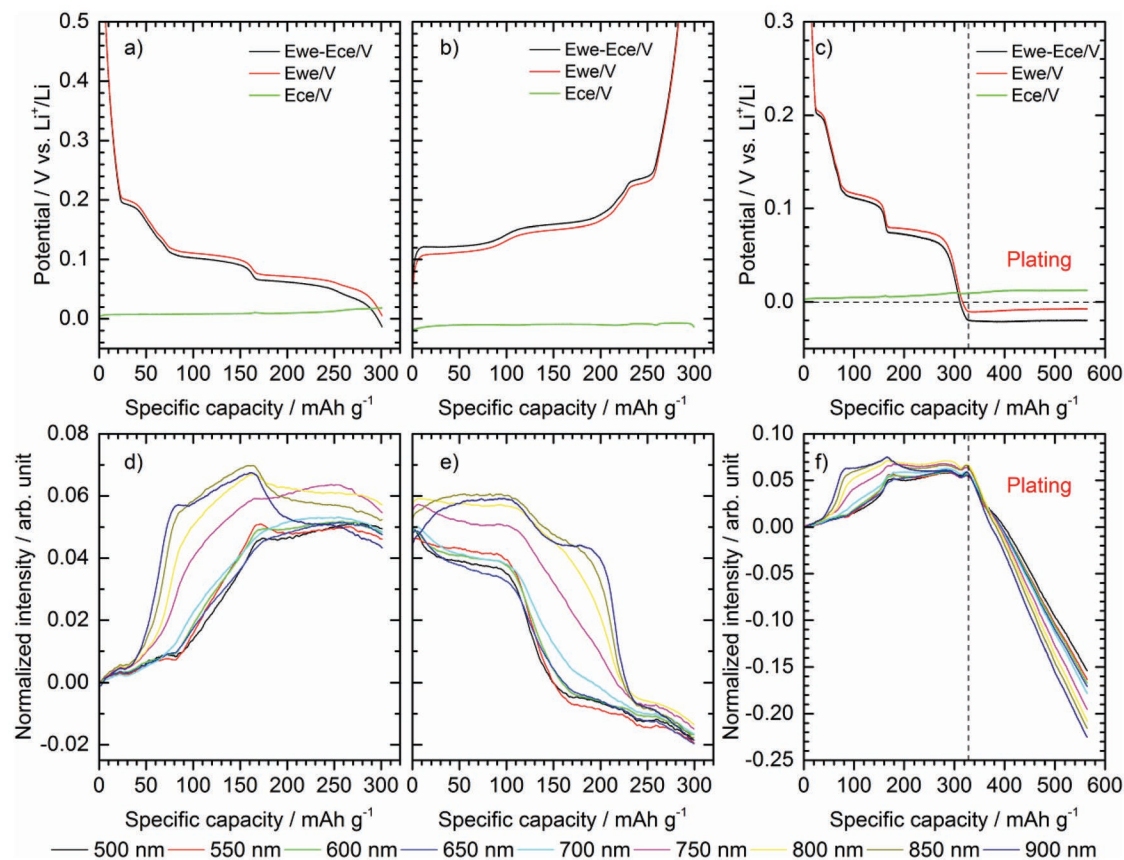


**Figure 2.** Cycling of graphite (WE) and lithium (CE) half-cell, including a piece of lithium as the reference electrode. The voltage profiles from the constant current ( $0.245\text{ mA cm}^{-2}$ , corresponding to 0.1 C) lithiation and delithiation are shown in (a) and (b), respectively. The corresponding normalized transmission intensities from the FOEW sensor are shown in (d,e). The cell was slowly (C/20) lithiated beyond the maximum available lithium storage capacity and the resulting voltage profiles during the intercalation and subsequent lithium deposition are presented in (c). The corresponding optical response is shown in (f) and the black dashed line in (c) and (f) is positioned at the lithium nucleation potential.

sensor is shown in Figure 2d,e. Depending on the wavelength, the normalized intensity increased up to  $\approx 4\text{--}6\%$  during the lithiation step and then decreased in a similar manner during the following delithiation. Clearly, the changes in the intensity align well with the potential steps representing the lithium staging. Color variations in the graphite upon the stepwise lithiation are well-known and have been demonstrated with several experimental techniques,<sup>[25,26]</sup> including FOEW-sensors,<sup>[14]</sup> and this will be discussed in more detail further below.

Following the last formation cycle, the graphite was over-lithiated at a rate of C/20 well beyond the maximum available capacity. After  $\approx 300\text{ mAh g}^{-1}$ , the graphite potential (Figure 2c) dropped below zero as the number of intercalation sites became limited. There was also a nucleation dip present in the potential, indicated by the dashed line in Figure 2c, and the plating then continued at a potential a few millivolts above the nucleation potential. The corresponding optical signal is shown in Figure 2f, and the change in the intensity during the intercalation part of the C/20 lithiation was as expected very similar to the intensity during the 0.1 C lithiation in the formation step (Figure 2d). As the maximum capacity was reached and the plating initiated according to the working electrode potential, there was a distinct drop in intensity at all wavelengths, and when the plating continued there was also a clear wavelength dependence in the optical response. These observations were in good agreement with the lithium plating experiment on copper above, as well as with previous work on sodium plating on either copper or hard carbon electrodes.<sup>[22]</sup> In Figure 2f, a small increase in the intensity was also present just before the onset of lithium plating, which again was observed for sodium plating on hard carbon electrodes, as well as for the longest wavelengths for the lithium plating on copper in Figure 1 above.

Post-mortem studies of the graphite lithiated beyond the available capacity clearly showed silvery lithium metal plated on the surface of the electrode (see Figure 3a). The deposited lithium was homogeneously distributed across the area facing the lithium counter electrode, except for a small trench where the optical fiber sensor was located. In the outer part of the graphite electrode not overlapping with the opposite lithium counter electrode the graphite showed a distinct golden appearance, indicating full lithiation. Furthermore, Figure 3b shows the side of the Celgard separator facing the glass fiber separator

and there was no trace of lithium present. The side of the glass fiber separator which was placed on top of the Celgard separator is shown in Figure 3c. Although there is some lithium captured in this separator it was caught from the lithium CE side. Post-mortem images also showed that some of the graphite coatings had been scuffed off around the edge of the electrode during the manual punching of the electrode foils (see Figure 3a and Figure S2, Supporting Information), exposing the copper substrate. It also looked like the coating in this region had delaminated to some extent.

### 2.3. Polarisation-Induced Plating

Lithium plating on graphite can also be triggered by polarization as a result of excessive cycling rates. An experiment was set up where a graphite-lithium half-cell was lithiated at 4 C, a rate sufficiently high to induce plating. Before this, six formation cycles at 0.1 C were performed and the graphite was also delithiated at 0.1 C after the fast lithiation. When the lithiation rate was increased to 4 C, polarization was clearly present in both the working and counter electrode potentials (Figure 4a). The graphite electrode potential dropped below zero after only  $\approx 15\text{ mAh g}^{-1}$ , and the lithium staging was as expected not clearly observed. After about  $120\text{ mAh g}^{-1}$  (indicated by a vertical dashed line in the figure), the lithiation proceeded at a higher potential which indicated the onset of plating. Although there was no clear nucleation dip (the WE potential was almost the same between  $100\text{--}140\text{ mAh g}^{-1}$ ), the result in Figure 4a shows that plating started long before the graphite was fully lithiated.

The corresponding optical response is presented in Figure 4b. Initially, the intensity increased as a result of the lithiation of the graphite (the change in intensity had similarities to the 0.1 C lithiation from the formation cycle in Figure 2d). As the capacity reached  $\approx 60\text{ mAh g}^{-1}$ , the intensity at all wavelengths began to decrease significantly, with the intensity at longer wavelengths decreasing more than at shorter wavelengths, which from the results above is a clear sign of lithium plating. In this experiment, however, lithium ions continue to intercalate into the graphite during plating and the electrochromic properties of the graphite hence most likely continue

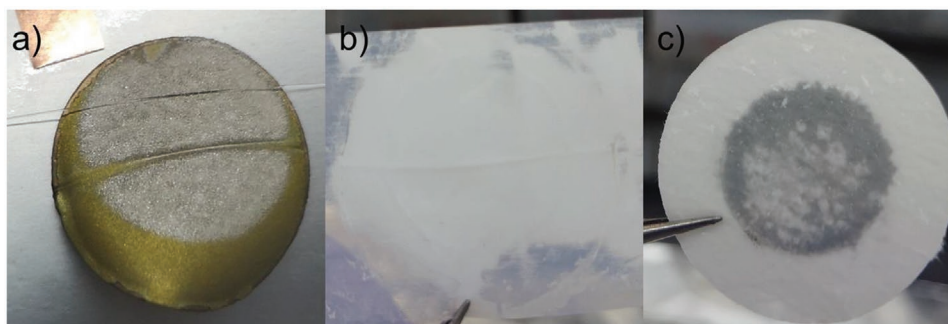


**Figure 3.** Post-mortem images of the graphite half-cell that was lithiated at C/20 beyond the maximum available capacity. a) shows the graphite WE with lithium metal clearly plated at the surface, and the outer part of the graphite shows a golden color. b) depicts the Celgard separator which was placed on top of the graphite electrode and the FOEW sensor. The side of the glass fiber separator that was placed towards the Celgard separator is shown in (c), lithium was clearly present but this originated from the lithium counter electrode.

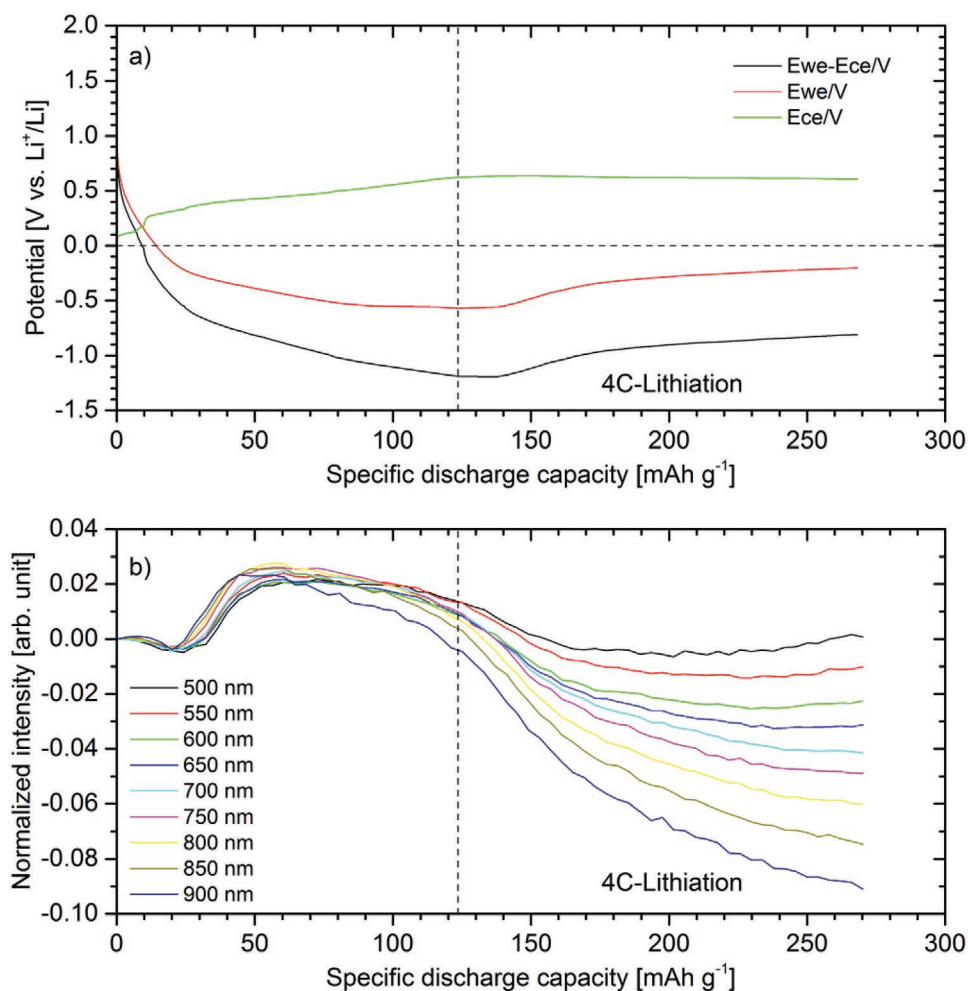


**Figure 4.** Polarization-induced lithium plating at the graphite electrode. The voltage profiles during the 4 C lithiation are shown in (a), and the corresponding intensity from the FOEW sensor is shown in (b). The 4 C lithiation was capacity limited and terminated when approximately 77% of the available capacity was reached, and the dashed line is positioned at the minimum in the graphite potential.

to contribute to the intensity. Compared to the plating as a result of the over-lithiation of the graphite in Figure 2f, there is also a much more negative potential for the graphite electrode in Figure 4a, which is an important factor for the plating conditions. A more complicated optical response from the fiber optical sensor was also experienced for the combined fast sodiation and sodium plating in the previous hard carbon experiments.<sup>[22]</sup> Nevertheless, the optical response indicated the plating of lithium before there was a minimum in the graphite potential. The use of a fiber optical sensor in a cell may hence serve as an early warning sign to reduce the risk of harmful plating.

Disassembly of the cell also confirmed the presence of lithium on the graphite electrode even though the capacity was limited conservatively and the graphite was delithiated at 0.1 C following the 4 C lithiation (see Figure 5a). The deposited lithium had a grey appearance as compared to the silvery lithium metal seen in Figure 3a (which was observed directly after lithiation). The Celgard separator which was placed in direct contact with the graphite working electrode (see Figure 5b) also showed a black discoloration and traces

of lithium. From the glass fiber separator, showing the side placed towards the Celgard separator, grey lithium dendrites most likely originating from the CE side could clearly be seen (Figure 5c).

#### 2.4. Detection of Graphite Staging

The electrochromic properties of graphite upon (de)lithiation are well known and will also influence the light modulation at the optical fiber. As a consequence, the results in Figure 2a,b,d,e, showed a clear correlation between the optical response from the graphite electrode and the graphite potential during the slow (de)lithiation. This was different compared to the slow (de)sodiation of hard carbon, which did not change the intensity much.<sup>[22]</sup> The stepwise drop in the graphite potential is a result of the lithiation mechanism, described as staging already in 1938.<sup>[24]</sup> Briefly, the staging model describes the periodic sequence of lithiated and non-lithiated graphene layers. Associated with the staging is also a color change of the graphite, a consequence of changes in the electronic band

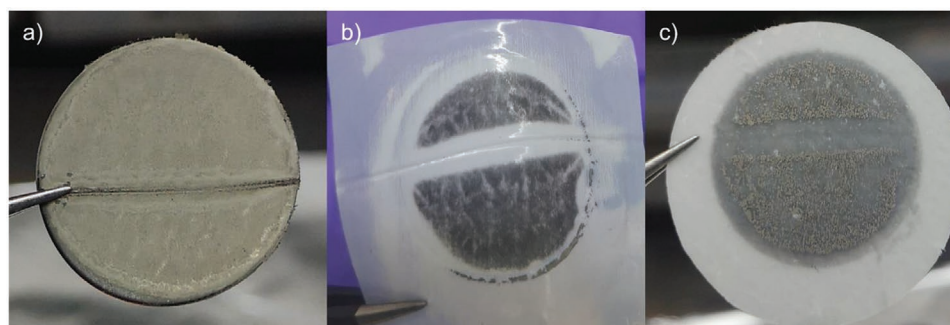


**Figure 5.** Post-mortem images of the graphite half-cell. a) Graphite electrode which was delithiated following the fast lithiation at 4 C. From the image it is also clear where the optical fiber was positioned. b) Celgard separator showing traces of plating (the side that was facing the graphite electrode). c) Glass fiber separator showing the side that was placed towards the Celgard separator, grey lithium dendrites were clearly visible.

structure.<sup>[26]</sup> According to the model, in stage IV there are three empty graphene layers between every lithiated layer, until stage I where all graphene layers are lithiated, and the corresponding colors<sup>[14,26]</sup> are graphite-like, blue, red, and golden, respectively. The staging and color changes have been studied with a wide range of methods,<sup>[24]</sup> resulting in important information on the lithiation mechanism. Optical fibers incorporated in battery cells also provide benefits when analyzing stepwise lithiation. The fiber can be placed directly on the anode surface for in situ spectroscopic analysis, and the required equipment is relatively simple and cheap. Nieva et al.<sup>[14]</sup> reported the use of in situ FOEW spectroscopy to analyze the lithiation of graphite (extracted from a commercial anode) in a Swagelok cell, and concluded that the intensity from the fiber closely followed the reflectance of graphite. They also demonstrated the possibility to estimate the SOC via the optical fiber and concluded that the SOC estimation was particularly sensitive in the near IR region.

In this contribution, the aim was also to demonstrate that FOEW spectroscopy could be employed to follow the staging in-operando in a commercial-like pouch cell battery, from delithiated graphite to over-lithiation leading to the plating. In **Figure 6**, the transition between stages and LiC-compositions is indicated in both the graphite potential and the response from the sensor. It is clearly seen that the stages can be identified also in the optical response from the fiber. From **Figure 6**, it also seen that the intensity changes are higher for the longest wavelengths (near infrared) during the early stages of lithiation, which are in line with the findings from Nieva et al.<sup>[14]</sup> It should, however, be remembered that the input from the fiber only reflects the optical properties of the surface of the graphite particles, and only those situated close to the sensing region of the fiber. This can, on the other hand, be an advantage if the purpose is to analyze the optical properties of the graphite at a specific spot in a cell. Compared to analyzing the graphite potential, the fiber optical sensor may also be a better option if a proper reference electrode cannot be included in the cell, or if the provided voltage is based on the contribution from several cells. From **Figure 4** it could also be concluded that the staging at a high C-rate was not clearly seen in the intensity (nor in the graphite potential). With respect to the fiber optical sensor, this is most likely explained by the fact that the surface of the graphite particles near the sensing region seems to be almost fully lithiated already at  $\approx 50$  mAh g<sup>-1</sup>. Future work will

reveal if FOEW spectroscopy experiments will bring some valuable in operando information to enhance the understanding of the lithiation mechanism, or to improve the estimation of the SOC during battery operation.

To summarize, the correlation between the fiber optical signal and the lithium plating was thus found to be similar compared to previous experiments on sodium plating in sodium-ion batteries. As described in more detail elsewhere,<sup>[22]</sup> the original fiber cladding was removed before the incorporation of the fiber optical sensor in the pouch cell, hence the electrolyte and nearby graphite particles in the very close vicinity of the fiber will act as the new cladding.<sup>[16]</sup> In the optical fiber, light is guided via total internal reflection at the interface between the core and the cladding, and at each point of reflection, an evanescent wave is formed that penetrates into the cladding. Although the amplitude of the evanescent waves decreases rapidly from the interface, they still interact with the surrounding medium. If the medium is lossy, the evanescent waves can be absorbed, and the light intensity from the fiber will be attenuated accordingly. When lithium is deposited close to the fiber, the conditions at the interface will change significantly as a new cladding will be established, and more light will be lost from the optical fiber. The latter is based on the fact that metals generally show a high reflectance<sup>[22,27]</sup> in the visible spectral region. The correlation between the fiber optical sensor and the lithium plating is hence dependent on how strongly lithium modulates the light at the fiber interface, in addition to the number of reflections per unit length, and the penetration depth of the evanescent waves.<sup>[28,29]</sup> In the experiments it was also found that the fiber optical signal decreased more for the longer wavelengths during lithium plating on both copper and graphite electrodes. This is most likely related to the larger penetration depth for the longer wavelengths.<sup>[22]</sup> Further investigations are motivated to enhance the understanding of exactly how the lithium modulates the light, and also how the size of the lithium nuclei and their distribution on the graphite surfaces influence the fiber optical signal. It should also be remembered that the deposited lithium also contains reaction products from the reduction of the electrolyte (i.e., a solid electrolyte interphase [SEI]). This was also confirmed by the diffuse gray appearance from the post-mortem images. It was also shown that the fiber optical sensor could follow the electrochromic properties of the graphite upon (de)intercalation

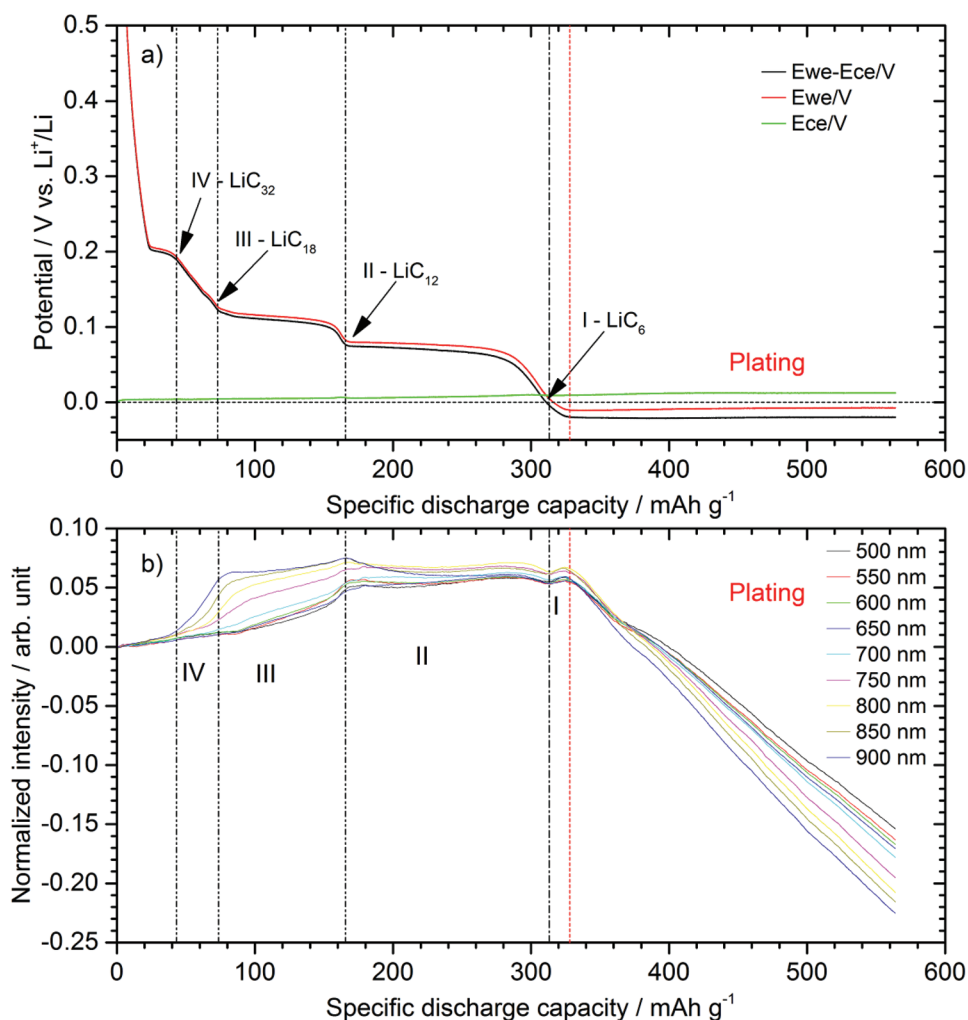


**Figure 6.** Lithiation of graphite (WE) in a half-cell with a lithium counter electrode (CE), including a piece of lithium as the reference electrode. The voltage profiles from the C/20 lithiation are shown in (a), and the normalized transmission intensities from the FOEW sensor during the lithiation are shown in (b) (data from Figure 2c,f, respectively). The lithiation stages I–IV and the LiC-compositions are indicated. The red dashed line is positioned at the lithium nucleation potential, while the dashed black lines indicate the transitions.

of lithium ions. Although the color change in the graphite had a subtler influence on the fiber optical signal, it was possible to follow the lithium staging in-operando in the pouch cells. However, the combined influence on the intensity from both the intercalation and plating at higher rates was found to complicate the elucidation of the point where the plating was initiated.

### 3. Conclusion

A fiber-optic evanescent wave sensor was used to demonstrate the in operando detection of lithium plating on graphite electrodes. The deposition of lithium on the graphite was found to significantly modulate the light at the sensing region of the optical fiber and was demonstrated for intentional plating on bare copper as well as for plating on graphite electrodes induced by over-lithiation and a too-high cycling rate. It was, for example, shown that the plating resulted in a loss of light from the optical fiber, and there was also a small pre-nucleation

increase in the intensity which may serve as an early warning sign for lithium dendrite formation. In general, the results were also found to correlate well with previous experiments on the detection of sodium plating on both copper and hard carbon electrodes. Furthermore, the sensor also allowed in-operando monitoring of the lithium staging in the graphite electrode during (de)intercalation of lithium ions.

Although a fiber optical sensor might not be easily incorporated in commercial batteries, the input from a sensor may provide a BMS with additional information to reduce the risk of harmful lithium plating, for example from a specific part of a cell or in a cell where a proper reference electrode cannot be included. The wavelength dependence may also bring additional information. Further investigations, for example, including control of the size and distribution of the lithium nuclei, are needed to better understand how the early stages of lithium nucleation modulate the light, especially at higher lithiation rates. In addition, further experiments should also be focused on the possibility to employ FOEW spectroscopy

to analyze the presence of dead lithium on the anode surface and link that to the aging of the cell, and the possibility to use FOEW spectroscopy in the development of so-called anode free batteries.

## 4. Experimental Section

**Optical Sensor Preparation and Sensor Integration:** The fiber optic evanescent wave sensor was prepared by fusion splicing each end of a coreless optical fiber (FG125LA, Thorlabs) with a diameter of 125  $\mu\text{m}$  to standard step-index multimode optical fibers (FG105LCA, Thorlabs), with a cladding diameter of 125  $\mu\text{m}$  and a core diameter of 105.5  $\mu\text{m}$ . The detailed preparation and integration of the sensors followed the same procedure previously described in ref. [22]. The FOEW sensors had a final sensing length of 25 mm and were inserted into three-electrode pouch cells in a transmission configuration. Battery assembly was done inside an argon-filled glovebox and the sensor was positioned at the surface of the working electrode in all half-cells. To ensure a hermetic seal around the optical fiber entry and exit points, the extra heat-sealing film was applied around the edges of the pouch cells.

**Cell Preparation:** All pouch cells were prepared as three-electrode pouch cells with integrated FOEW sensors in a half-cell configuration closely following the experimental procedure of our previous work.<sup>[22]</sup> Half-cells using metallic lithium as both the counter electrode and the reference electrode were assembled for lithium plating experiments on copper and graphite electrodes (see Scheme S1, Supporting Information). Copper electrodes were prepared by punching 20 mm disks from high-quality copper foil, which was cleaned by ultrasonication in ethanol for 30 min, and vacuum-dried in a vacuum oven for 12 h at 110 °C inside an argon-filled glovebox. Graphite electrodes were either punched into 20 mm disks or laser cut to 21 mm in diameter from commercial graphite electrode foils (10 010 013, Customcells), having an area capacity of 2.46 ( $\pm 0.1$ ) mAh cm<sup>-2</sup> and a specific capacity of 355 mAh g<sup>-1</sup>. Metallic lithium counter electrodes and reference electrodes were prepared from metallic lithium foil (125  $\mu\text{m}$ , China Energy Lithium CO. Ltd) by punching 20 mm disks while the reference electrodes (used in all cells) were made by cutting small pieces of lithium from the foil. All handling of metallic lithium was carried out in an argon-filled glovebox. Commercially available 1 M lithium hexafluorophosphate in ethylene carbonate:diethyl carbonate (1:1 vol.%) (Solvionic) was used as an electrolyte in all cells, and they were assembled with a combination of (Celgard, 2325) and glass fiber (Whatman, GF/A) separators. The Celgard separator was cut to approximately 2 × 2 cm, dried under vacuum for 5 h at 70 °C, and placed on top of the graphite electrode with the FOEW sensor during assembly. The glass fiber separators were punched into 30 mm disks, which were dried for 12 h at 110 °C under vacuum and placed on top of the Celgard separator with the lithium reference electrode, placed close to the electrode stack and sandwiched in between. All cells were assembled using 300  $\mu\text{L}$  electrolyte added to the separators and vacuum sealed under argon.

**Electrochemical Characterization:** All experiments were carried out using galvanostatic cycling on a Biologic VMP2 multichannel potentiostat/galvanostat in a cleanroom environment with a controlled room temperature of 21  $\pm$  1 °C. For lithium plating and stripping experiments on copper-lithium half-cells, galvanostatic cycling was performed using a current of approximately 0.123 mA cm<sup>-2</sup>, corresponding to a rate of C/20 based on the capacity of a graphite electrode of equal size. The cycling was performed between -0.5 and 1.6 V and the charge and discharge were both limited to 30 min. Graphite-lithium half-cells were precycled at 0.1 C during 4–6 cycles between 0.005 and 1.6 V, before slowly lithiating the graphite at a constant current of C/20. The rates were calculated based on the area capacity of the graphite electrode foils (Customcells) and the final capacity determined from the total weight of the electrode, the weight of the copper substrate, the given specific capacity of the graphite electrodes, and the amount of active material. In addition, graphite-lithium half-cells were also discharged at 4 C following

the formation cycling at 0.1 C. The 4 C discharge was capacity-limited and terminated when approximately 77% of the available lithium storage space based on the sixth formation cycle was reached ( $\approx 268$  mAh g<sup>-1</sup>). To provide a uniform pressure distribution across the cells, they were clamped using a layer of EPDM foam on either side of the pouch cell.

**Optical-Electrochemical Setup and Optical Measurement:** The three-electrode pouch cells with integrated FOEW sensors were connected to an optic unit (Insplorion AB) having a stabilized broadband light source and a spectrometer operating in the UV–vis–NIR spectral range. The fiber optic sensor was connected to the light source and the spectrometer in transmission configuration using multimode patch cables with standard FC/PC to SMA-905 connections, while the pouch cell was connected to the battery cyclers. The sampling period of the spectrometer was set to 10 s for all experiments except for the lithium plating and stripping experiments on copper electrodes, where a faster sampling rate of 1 s was chosen. The charge-coupled device (CCD) detector of the spectrometer collected spectra in the range of 400–1000 nm, averaging 200 spectra for each sampling period while cycling the battery cells (based on the intensity from the light source only 500–900 nm was used). The dark noise contribution was subtracted from the spectra prior to further analysis of the optical signal. The transmission intensities were subtractively normalized according to  $\Delta I/I_0 = (I - I_0)/I_0$ , where  $I$  is the intensity at each specific wavelength during cycling, and  $I_0$  is the corresponding intensity at the beginning of lithiation of the graphite electrode. A Savitsky–Golay filter was applied for post-processing of the optical signal to further reduce noise and increase precision without distorting the signal.

## Supporting Information

Supporting Information is available from the Wiley Online Library or from the author.

## Acknowledgements

StandUp for Energy, Skellefteå Kraft, and Batteries Sweden (BASE)/Vinnova (project no. 2019-00064) are gratefully acknowledged for financial support. Insplorion AB are also acknowledged for support with optical equipment.

## Conflict of Interest

The authors declare no conflict of interest.

## Data Availability Statement

The data that support the findings of this study are available from the corresponding author upon reasonable request.

## Keywords

detection, evanescent waves, fiber optical sensor, graphite, lithium plating

Received: July 27, 2022  
Revised: October 3, 2022  
Published online: December 1, 2022

- [1] Y. D. Su, Y. Preger, H. Burroughs, C. Sun, P. R. Ohodnicki, *Sensors* **2021**, *21*, 1397.  
[2] L. H. J. Raijmakers, D. L. Danilov, R.-A. Eichel, P. Notten, *Appl. Energy* **2019**, *240*, 918.

- [3] C. Grey, J.-M. Tarascon, *Nat. Mater.* **2017**, *16*, 45.
- [4] R. Raccichini, M. Amores, G. Hinds, *Batteries* **2019**, *5*, 12.
- [5] W. Waag, C. Fleischer, D. U. Sauer DU, *J. Power Sources* **2014**, *258*, 321.
- [6] A. G. Hsieh, S. Bhadra, B. J. Hertzberg, P. J. Gjeltema, A. Goy, J. W. Fleisher, D. A. Steingart, *Energy Environ. Sci.* **2015**, *8*, 1569.
- [7] J. Huang, S. T. Boles, J.-M. Tarascon, *Nat. Sustain.* **2022**, *5*, 194.
- [8] M. Dotoli, R. Rocca, M. Giuliano, G. Nicol, F. Parussa, M. Baricco, A. M. Ferrari, C. Nervi, M. F. Sgroi, *Sensors* **2022**, *22*, 1763.
- [9] A. Ghannoum, P. Nieva, *J. Energy Storage* **2020**, *28*, 101233.
- [10] J. Huang, L. Albero Blanquer, J. Bonefacino, J. E. R. Logan, D. A. Dalla Corte, C. Delacourt, B. M. Gallant, S. T. Boles, J. R. Dahn, H. Y. Tam, J. M. Tarascon, *Nat. Energy* **2020**, *5*, 674.
- [11] R. Wang, H. Zhang, F. L. Q. Liu, X. Han, X. Liu, K. Li, G. Xiao, J. Albert, X. Lu, T. Guo, *Nat. Commun.* **2022**, *13*, 547.
- [12] C. Gardner, E. Langhammer, W. Du, D. J. L. Brett, P. R. Shearing, A. J. Roberts, T. Amietszajew, *Sensors* **2022**, *22*, 738.
- [13] A. Ghannoum, P. Nieva, A. Yu, A. Khajepour, *ACS Appl. Mater. Interfaces* **2017**, *9*, 41284.
- [14] A. Ghannoum, R. C. Norris, K. Iyer, L. Zdravkova, A. Yu, P. Nieva, *ACS Appl. Mater. Interfaces* **2016**, *8*, 18763.
- [15] L. Hedman, D. Nilebo, E. Larsson Langhammer, F. Björefors, *ChemSusChem* **2020**, *13*, 5731.
- [16] J. Hedman, F. Björefors, *ACS Appl. Energy Mater.* **2022**, *5*, 870.
- [17] W. Cai, C. Yan, Y.-X. Yao, L. Xu, X.-R. Chen, J.-Q. Huang, Q. Zhang, *Angew. Chem., Int. Ed.* **2021**, *60*, 13007.
- [18] A. M. Tripathi, W.-N. Su, B. J. Hwang, *Chem. Soc. Rev.* **2018**, *47*, 736.
- [19] T. Waldmann, B.-I. Hogg, M. Wohlfahrt-Mehrens, *J. Power Sources* **2018**, *384*, 107.
- [20] J. Luo, C.-E. Wu, L.-Y. Su, S.-S. Huang, C.-C. Fang, Y.-S. Wu, J. Chou, N.-L. Wu, *J. Power Sources* **2018**, *406*, 63.
- [21] D. Rehnlund, C. Ihrfors, J. Maibach, L. Nyholm, *Mater. Today* **2018**, *21*, 1010.
- [22] J. Hedman, R. Mogensen, R. Younesi, F. Björefors, *ACS Appl. Energy Mater.* **2022**, *5*, 6219.
- [23] A. Mohammadi, L. Monconduit, L. Stievano, R. Younesi, *J. Electrochem. Soc.* **2022**, *169*, 070509.
- [24] J. Asenbauer, T. Eisenmann, M. Kuenzel, A. Kazzazi, Z. Chen, D. Bresser, *Sustainable Energy Fuels* **2020**, *4*, 5387.
- [25] Y. Chen, K.-H. Chen, A. J. Sanchez, E. Kazyak, V. Goel, Y. Gorlin, J. Christensen, K. Thornton, N. P. Dasgupta, *J. Mater. Chem. A* **2021**, *9*, 23522.
- [26] P. Maire, A. Evans, H. Kaiser, W. Scheifele, P. Novák, *J. Electrochem. Soc.* **2008**, *155*, A862.
- [27] M. Fox, *Optical Properties of Solids*, 2nd ed., Oxford Master Series in Condensed Matter Physics, Oxford University Press, Oxford **2010**.
- [28] V. Ruddy, B. D. MacCraith, J. A. Murphy, *J. Appl. Phys.* **1990**, *67*, 6070.
- [29] S. K. Khijwania, B. D. Gupta, *Opt. Quantum Electron.* **1999**, *31*, 625.